

Topological edge states in single- and multi-layer Bi_4Br_4

Jin-Jian Zhou,¹ Wanxiang Feng,² Gui-Bin Liu,² and Yugui Yao^{2,1, a)}

¹⁾*Institute of Physics, Chinese Academy of Sciences and Beijing National Laboratory for Condensed Matter Physics, Beijing 100190, China*

²⁾*School of Physics, Beijing Institute of Technology, Beijing 100081, China*

(Dated: 29 February 2024)

Topological edge states at the boundary of quantum spin Hall (QSH) insulators hold great promise for dissipationless electron transport. The device application of topological edge states has several critical requirements for the QSH insulator materials, e.g., large band gap, appropriate insulating substrates, and multiple conducting channels. In this paper, based on first-principle calculations, we show that Bi_4Br_4 is a suitable candidate. Single-layer Bi_4Br_4 was demonstrated to be QSH insulator with sizable gap recently. Here, we find that, in multilayer systems, both the band gaps and low-energy electronic structures are only slightly affected by the interlayer coupling. On the intrinsic insulating substrate of Bi_4Br_4 , the single-layer Bi_4Br_4 well preserves its topological edge states. Moreover, at the boundary of multilayer Bi_4Br_4 , the topological edge states stemming from different single-layers are weakly coupled, and can be fully decoupled via constructing a stair-stepped edge. The decoupled topological edge states are well suitable for multi-channel dissipationless transport.

PACS numbers: 73.22.-f, 73.43.-f, 71.70.Ej, 85.75.-d

The hallmark of quantum spin Hall (QSH) insulators, also known as two-dimensional (2D) topological insulators, is the gapless helical edge states inside the bulk band gap^{1,2}. Along a given edge of QSH insulator, a pair of edge states with opposite spins propagate in opposite directions, and they are topologically protected against backscattering from non-magnetic disorder. With this novel property, topological edge state promises its application to dissipationless transport, which has been demonstrated experimentally in HgTe/CdTe ³ and InAs/GaSb ⁴ quantum wells. Despite the great promise, the device application of topological edge state has been hampered by the lack of suitable materials that meet several critical requirements, e.g., large band gap for room temperature applications, and multiple conducting channels for high signal-to-noise ratio.

Inspired by the discovery of graphene, 2D materials with atomic thickness have become an emerging playground for exploring novel physics. The QSH effect was firstly predicted in graphene⁵, in which the band gap opened by spin-orbital coupling (SOC) is extremely small⁶. Subsequently, some honeycomb-like materials with heavier elements were proposed to be QSH insulators with experimental accessible gaps, such as silicene⁷ and $\text{Bi}(111)$ bilayer⁸. However, the lack of appropriate insulating substrates becomes another crucial issue. The QSH phase of 2D materials may be destroyed due to its interaction with substrates⁹. Even the QSH phase survives, the hybridization between the topological edge states and the substrate's bulk states is disturbing^{10,11}. Topological edge modes of Bi-bilayer on the surface of Bi single crystal were detected by STM recently¹², thanks to that the edge states of certain edge type are only slightly hybridized with bulk Bi. Yet the metallic sur-

face of bulk Bi is inadequate for edge state transport. Other newly proposed QSH insulators with sizable band gaps, such as single-layer Bi_4Br_4 ¹³ and transition metal dichalcogenides¹⁴, may break this obstruction because their bulk crystals are insulators.

In this paper, based on first-principles calculations, we study the effect of interlayer coupling on the electronic structures and edge states of multilayer Bi_4Br_4 . We find that the band gaps of multilayer Bi_4Br_4 hardly changes as the number of layers increasing, and the interlayer coupling has small impact on the low-energy electronic structures of multilayer Bi_4Br_4 , which is attributed to the special orbital character of the band edges. Therefore, the surface of bulk Bi_4Br_4 can be an intrinsic insulating substrate for the SL Bi_4Br_4 . With this substrate, the Fermi velocity of topological edge states is slightly reduced compared to the freestanding case. Moreover, at the boundary of multilayer Bi_4Br_4 , the topological edge states stemming from different single-layers are weakly coupled, which can be further decoupled by constructing a stair-stepped edge. The decoupled topological edge states can serve as multiple conducting channels. Our results indicate that the Bi_4Br_4 is an excellent candidate for manufacturing multi-channel dissipationless electron device.

First principle calculations are carried out using the projector augmented wave method¹⁵ as implemented in the Vienna *ab initio* simulation package¹⁶. Both the Perdew-Burke-Ernzerhof generalized gradient approximation (GGA)¹⁷ and the Heyd-Scuseria-Ernzerhof hybrid functional (HSE06)¹⁸ are used for the exchange-correlation potential. The ionic position are relaxed employing the van der Waals (vdW) corrections^{19,20}. Maximally localized Wannier functions (MLWFs) for the *p*-orbitals of Bi and Br atoms are constructed using the WANNIER90 code²¹. In the HSE06 calculations, the surface electronic structures are calculated using the combination of MLWFs and surface Green's function

^{a)}Electronic mail: yg Yao@bit.edu.cn

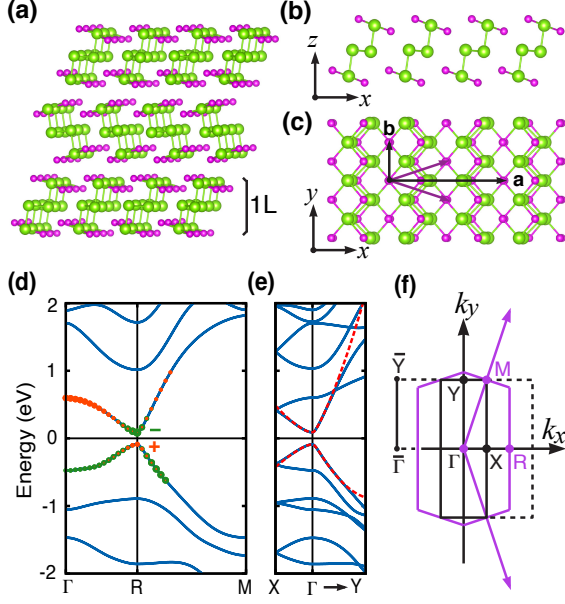


FIG. 1. Side view of (a) multilayer and (b) SL Bi_4Br_4 with green (small purple) balls representing Bi (Br). Bi atoms in the middle of SL are labeled as Bi_{in} , while these bonded with Br are labeled as Bi_{ex} . (c) Top view of SL Bi_4Br_4 . The black (purple) vectors are lattice vectors of conventional (primitive) unit cell. (d) HSE06 band structure of SL Bi_4Br_4 with orbital projected character in the low-energy region. The size of orange and green circle denote the weight of $\text{Bi}_{ex}-p_x$ and $\text{Bi}_{in}-p_x$ orbital projections, respectively. (e) Comparison of band structures under conventional cell from HSE06 calculation (blue line) and the fitted $k \cdot p$ Hamiltonian (red dashed line). (f) the Brillouin Zones of primitive (purple) and conventional cell (black). When conventional cell is adopted, the Brillouin Zone of primitive cell is folded, e.g., the R point under primitive cell is folded to the Γ point under conventional cell.

methods²².

Bi_4Br_4 has a layered structure^{23,24}, as shown in Fig. 1(a). Within each single-layer (SL), one Bi atomic layer is sandwiched by two Bi/Br atomic layers. The normal and mirror-reflected SLs are stacked alternatively along the z direction with the interactions between adjacent SLs of weak vdW-type. A SL of Bi_4Br_4 has a thickness of ~ 7 Å. It can be regarded as a parallel arrangement of one-dimensional (1D) infinite molecule chains [Fig. 1(b)]. From the top view shown in Fig. 1(c), one can see that the SL structure belongs to the centered rectangular lattice, whose primitive unit cell is half size of its conventional cell. The conventional unit cell consists of two 1D chains, and the lattice constants a and b are 13.064 Å and 4.338 Å, respectively²³.

The SL Bi_4Br_4 has been predicted to be QSH insulator in our recent work¹³. In the absence of SOC, the top of valence band (TVB), dominated by $\text{Bi}_{in}-p_x$ orbital, has odd parity under inversion symmetry; while the bottom of conduction band (BCB), dominated by $\text{Bi}_{ex}-$

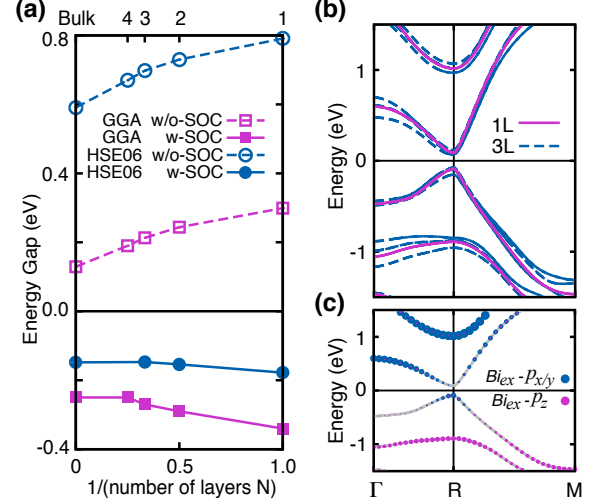


FIG. 2. (a) The dependence of energy gap of few-layer Bi_4Br_4 on the number of layers calculated by using GGA and HSE06 potentials. (b) Comparison between HSE06 band structures of single-layer and triple-layer Bi_4Br_4 . (c) HSE06 band structures of SL Bi_4Br_4 with orbital projected character. The size of blue (purple) circle denotes the weights of $\text{Bi}_{ex}-p_{x/y}$ ($\text{Bi}_{ex}-p_z$) orbital projections.

p_x orbital, has even parity¹³. After turning on SOC, as shown in Fig. 1(d), both the orbital character and parity of the band edges are inverted at the R point due to the strong SOC of Bismuth. This band inversion result in non-trivial topological phase ($\mathbb{Z}_2 = 1$) in SL Bi_4Br_4 .

From SL to multilayer system, the significant electronic properties may be altered by interlayer coupling, e.g., the direct to indirect band gap transition between monolayer and multilayer MoS_2 ²⁵. To study the effect of interlayer coupling on electronic structure of Bi_4Br_4 , especially for the inverted band gap, we calculate the band structures of few-layer Bi_4Br_4 using both GGA and HSE06 potentials. The calculated band gaps of Bi_4Br_4 from SL to bulk systems are shown in Fig. 2(a). In the absence of SOC, the band gaps of HSE06 are obviously larger than those of GGA. This is because the GGA calculation usually underestimates the band gap²⁶. In both GGA and HSE06 calculations, the band gap slightly decreases as the number of layers increasing, and the differences of band gaps are within ~ 0.2 eV. When SOC is turned on, the band gaps of multilayer Bi_4Br_4 are inverted in the similar way as SL system. The inverted band gaps are presented with negative values in Fig. 2(a). The dependence of band gap on the number of layers is further reduced. For HSE06 result, the band gap difference between SL and bulk systems is only within ~ 30 meV, which is a very small value compared to other layered materials, e.g., black phosphorus (~ 0.7 eV)²⁷.

Apart from the band gaps, the low-energy electronic structures are also insensitive to the interlayer coupling. Fig. 2(b) shows the comparison between HSE06 band

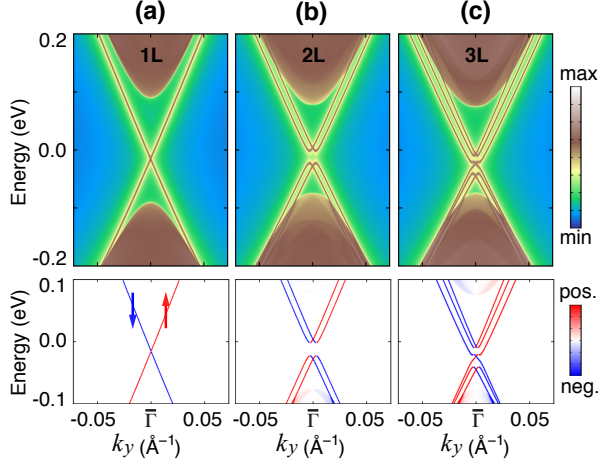


FIG. 3. The edge density of states (first row) and spin polarization (second row) of (a) single-layer, (b) double-layer, and (c) triple-layer Bi_4Br_4 . The Fermi level is set to the bulk band gap center.

structures of SL and triple-layer Bi_4Br_4 . The band features are essentially the same for both systems. Each band in SL Bi_4Br_4 corresponds to three bands in triple-layer Bi_4Br_4 , which are split due to the interlayer coupling. As can be seen in Fig. 2(b), The band splitting around Fermi-level is rather small, e.g., the band splitting of BCB (TVB) is about 40 (80) meV.

The small band splittings can be attributed to the special orbital characters of the band edges. When SLs are stacked together to form a multilayer structure, the states dominated by orbitals with larger interlayer hopping usually have larger band splitting in multilayer systems. Obviously, the out-of-plane p_z orbital has larger interlayer hopping compared to the in-plane $p_{x/y}$ orbitals, and the orbitals from Bi_{ex} have larger interlayer hopping compared to those from Bi_{in} . The band structure of SL Bi_4Br_4 with orbital projected characters is plotted in Fig. 2(c). The second valence bands are dominated by $\text{Bi}_{ex}-p_z$ orbital, thus have relatively large band splitting of a few hundred meV in triple-layer system [Fig. 2(b)]. In contrast, the low-energy bands are dominated by the in-plane $p_{x/y}$ orbitals, mainly $\text{Bi}_{in}-p_x$ [Fig. 1(d)], therefore they are less affected by the interlayer coupling.

In the weak coupling limit, the multilayer system can be regarded as simple stacking of many isolated SLs which have topological edge states at the boundaries. We now focus on the evolution of these topological edge states when a weak interlayer coupling is introduced, such as the case in multilayer Bi_4Br_4 . The edge electronic structures and spin polarizations for the SL, double-layer and triple-layer Bi_4Br_4 are shown in Fig. 3. Since the coupling between adjacent 1D chains is much weaker than the intra-chain bonding²³, atomically sharp edges along the 1D chain axis (y -direction) without dangling bond can be stabilized. We construct such edges as semi-infinite systems, for which the surface Green's functions

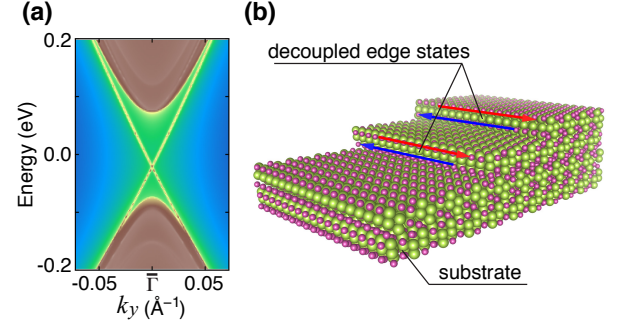


FIG. 4. (a) The density of states of Bi_4Br_4 with structures schematically plotted in (b).

are calculated. The energy and momentum dependent density of states, that are extracted from the imaginary part of the surface Green's function, are used to analyze the edge electronic structures. For SL Bi_4Br_4 [Fig. 3(a)], a single-Dirac-cone edges states linearly cross the bulk band gap. The Fermi velocity calculated by HSE06 is $\sim 6.5 \times 10^5 \text{ m}\cdot\text{s}^{-1}$, which is larger than the GGA result¹³. For double-layer Bi_4Br_4 [Fig. 3(b)], two pairs of topological edges states are weakly coupled, and a small gap of $\sim 20 \text{ meV}$ is opened. The gapped edge states indicate topological trivial phase in double-layer Bi_4Br_4 . For triple-layer Bi_4Br_4 [Fig. 3(c)], three pairs of topological edges states are coupled. However, there is one pair of edge states cross the band gap without gap opening, which indicates topological non-trivial phase in triple-layer Bi_4Br_4 . The difference of topological phase is because that the multilayer Bi_4Br_4 with even (odd) number of layers has even (odd) times of band inversions. The even times of band inversions result in a trivial insulator with $\mathbb{Z}_2 = 0$, while odd times of band inversions result in a QSH insulator with $\mathbb{Z}_2 = 1$.

Since the topological edge states are weakly coupled at the boundary of multilayer Bi_4Br_4 , they can be decoupled by constructing rough edge, such as a stair-stepped edge. We construct a two-layer Bi_4Br_4 film with stair-stepped edge supported by bulk Bi_4Br_4 surface, as plotted schematically in Fig. 4(b). With the step width of $\sim 5 \text{ nm}$, we calculate the energy spectrum of this system as shown in Fig. 4(a). The edge states linearly cross the bulk gap without gap-opening. Compared to the freestanding double-layer one [Fig. 3(b)], the topological edge states from the two different layers are fully decoupled at the stair-stepped edge, and the two single-Dirac-cones are degenerate. Another observation is that, due to the weak interaction with substrate, the Fermi velocity of the decoupled edge states ($\sim 5.6 \times 10^5 \text{ m}\cdot\text{s}^{-1}$) is a little smaller than that of the free standing SL system [Fig. 3(a)]. As the effect of interlayer coupling, the decreased Fermi velocity is also observed in the edge states of triple-layer systems.

To understand the essential physics, we develop a low-energy effective $k \cdot p$ Hamiltonian for SL Bi_4Br_4 by using

the theory of invariants, from which the effective Hamiltonian for the topological edge states can be further derived. For the convenience to construct natural edges along the 1D chain axis, we adopt the conventional unit cell. Consequently the band edges are folded to the Γ -point, as illustrated in Fig. 1(f). Both the BCB and TVB are double degenerate, and the two degenerate states are related by time reversal symmetry. Since the BCB (TVB) has odd (even) parity under inversion symmetry, we can denote these four states as $|-, \uparrow (\downarrow)\rangle$, $|+, \uparrow (\downarrow)\rangle$. By analyzing the inversion, mirror σ_h and time reversal symmetry, we can write down the low-energy effective Hamiltonian using the four states as basis (in the order of $|+, \uparrow\rangle$, $|-, \downarrow\rangle$, $|+, \downarrow\rangle$, $|-, \uparrow\rangle$)

$$H_{\Gamma}(k) = \epsilon_0(k) + \begin{pmatrix} M(k) & A_1 k_x & 0 & A_2 k_y \\ A_1^* k_x & -M(k) & A_2 k_y & 0 \\ 0 & A_2^* k_y & M(k) & -A_1^* k_x \\ A_2^* k_y & 0 & -A_1 k_x & -M(k) \end{pmatrix}$$

where $\epsilon_0(k) = C + D_1 k_x^2 + D_2 k_y^2$, $M(k) = M_0 - B_1 k_x^2 - B_2 k_y^2$. A_1 and A_2 are complex parameters, while the others are real parameters. By fitting the energy spectrum of the Hamiltonian with the HSE06 band structure [see Fig. 1(e)], we can determine these parameters as following: $C = 0.0$ eV, $D_1 = 0.506$ eV $\cdot\text{\AA}^2$, $D_2 = 4.82$ eV $\cdot\text{\AA}^2$, $M_0 = 0.09$ eV, $B_1 = 3.86$ eV $\cdot\text{\AA}^2$, $B_2 = 0.0032$ eV $\cdot\text{\AA}^2$, $A_1 = -1.81 + 0.046i$ eV $\cdot\text{\AA}$, $A_2 = -4.15 + 0.141i$ eV $\cdot\text{\AA}$. The band inversion can be produced by the fact of M_0 , B_1 , $B_2 > 0$. The form of the Hamiltonian is different from that of HgTe quantum well²⁸, but similar to that of Bi₂Se₃²⁹. In a similar way as for Bi₂Se₃, we can derive the effective Hamiltonian for the topological edge states.

$$H_{edge}(k_y) = |A_2| k_y \sigma_x$$

With the fitted value of A_2 , the Fermi velocity of the topological edge states is given by $\frac{|A_2|}{\hbar} \simeq 6.3 \times 10^5$ m \cdot s⁻¹, which is consistent with the HSE06 result [Fig. 3(a)]. The value of A_2 is modified when SL system is supported by Bi₄Br₄ surface. For the edge states of multilayer Bi₄Br₄, the effective Hamiltonian can be simply written by introducing coupling terms between $H_{edge}(k_y)$ of different SLs.

In summary, first-principle calculations demonstrate that both the band gaps and low-energy electronic structures of multilayer Bi₄Br₄ are little affected by the interlayer coupling. When SL Bi₄Br₄ is supported by the surface of bulk Bi₄Br₄, its topological edge states well survive except for a reduced Fermi velocity. Moreover, at the stair-stepped edge of multilayer Bi₄Br₄, the topological edge states from different SLs are fully decoupled. Our results indicate nano-fabrication on the cleaved surface of layered Bi₄Br₄ single crystal is adequate to realize multiple dissipationless conducting channels^{12,30}, hence Bi₄Br₄ is an excellent platform for

manufacturing QSH-based devices.

This work was supported by the MOST Project of China (Nos. 2014CB920903, 2013CB921903, 2011CBA00100), the NSF of China (Nos. 11174337, 11225418, 11374033, 11304014) and the SRFDPHE of China (No. 20121101110046, 20131101120052).

- ¹M. Z. Hasan and C. L. Kane, Rev. Mod. Phys. **82**, 3045 (2010).
- ²X.-L. Qi and S.-C. Zhang, Rev. Mod. Phys. **83**, 1057 (2011).
- ³M. König, S. Wiedmann, C. Brune, A. Roth, H. Buhmann, L. W. Molenkamp, X.-L. Qi, and S.-C. Zhang, Science **318**, 766 (2007).
- ⁴I. Knez, R.-R. Du, and G. Sullivan, Phys. Rev. Lett. **107**, 136603 (2011).
- ⁵C. L. Kane and E. J. Mele, Phys. Rev. Lett. **95**, 226801 (2005).
- ⁶Y. Yao, F. Ye, X.-L. Qi, S.-C. Zhang, and Z. Fang, Phys. Rev. B **75**, 041401 (2007).
- ⁷C.-C. Liu, W. Feng, and Y. Yao, Phys. Rev. Lett. **107**, 076802 (2011).
- ⁸S. Murakami, Phys. Rev. Lett. **97**, 236805 (2006).
- ⁹L. Chen, H. Li, B. Feng, Z. Ding, J. Qiu, P. Cheng, K. Wu, and S. Meng, Phys. Rev. Lett. **110**, 085504 (2013).
- ¹⁰T. Hirahara, G. Bihlmayer, Y. Sakamoto, M. Yamada, H. Miyazaki, S.-i. Kimura, S. Blügel, and S. Hasegawa, Phys. Rev. Lett. **107**, 166801 (2011).
- ¹¹F. Yang, L. Miao, Z. F. Wang, M.-Y. Yao, F. Zhu, Y. R. Song, M.-X. Wang, J.-P. Xu, A. V. Fedorov, Z. Sun, G. B. Zhang, C. Liu, F. Liu, D. Qian, C. L. Gao, and J.-F. Jia, Phys. Rev. Lett. **109**, 016801 (2012).
- ¹²I. K. Drozdov, A. Alexandradinata, S. Jeon, S. Nadj-Perge, H. Ji, R. J. Cava, B. Andrei Bernevig, and A. Yazdani, Nat Phys, (2014), DOI:10.1038/nphys3048.
- ¹³J.-J. Zhou, W. Feng, C.-C. Liu, S. Guan, and Y. Yao, Nano Letters **14**, 4767 (2014).
- ¹⁴X. Qian, J. Liu, L. Fu, and J. Li, arXiv:1406.2749 [cond-mat] (2014).
- ¹⁵P. E. Blöchl, Phys. Rev. B **50**, 17953 (1994).
- ¹⁶G. Kresse and J. Furthmüller, Phys. Rev. B **54**, 11169 (1996).
- ¹⁷J. P. Perdew, K. Burke, and M. Ernzerhof, Phys. Rev. Lett. **77**, 3865 (1996).
- ¹⁸J. Heyd, G. E. Scuseria, and M. Ernzerhof, J. Chem. Phys. **124**, 219906 (2006).
- ¹⁹M. Dion, H. Rydberg, E. Schröder, D. C. Langreth, and B. I. Lundqvist, Phys. Rev. Lett. **92**, 246401 (2004).
- ²⁰J. Klimeš, D. R. Bowler, and A. Michaelides, Phys. Rev. B **83**, 195131 (2011).
- ²¹A. A. Mostofi, J. R. Yates, Y.-S. Lee, I. Souza, D. Vanderbilt, and N. Marzari, Comput. Phys. Commun. **178**, 685 (2008).
- ²²M. P. L. Sancho, J. M. L. Sancho, J. M. L. Sancho, and J. Rubio, Journal of Physics F: Metal Physics **15**, 851 (1985).
- ²³E. V. Dikarev, B. A. Popovkin, and A. V. Shevelkov, Russ. Chem. Bull. Int. Ed. **50**, 2304 (2001).
- ²⁴T. G. Filatova, P. V. Gurin, L. Kloo, V. A. Kulbachinskii, A. N. Kuznetsov, V. G. Kytin, M. Lindsjö, and B. A. Popovkin, J. Solid State Chem. **180**, 1103 (2007).
- ²⁵K. F. Mak, C. Lee, J. Hone, J. Shan, and T. F. Heinz, Phys. Rev. Lett. **105**, 136805 (2010).
- ²⁶J. Heyd, J. E. Peralta, G. E. Scuseria, and R. L. Martin, The Journal of Chemical Physics **123**, 174101 (2005).
- ²⁷H. Liu, A. T. Neal, Z. Zhu, Z. Luo, X. Xu, D. Tomnek, and P. D. Ye, ACS Nano **8**, 4033 (2014).
- ²⁸B. A. Bernevig, T. L. Hughes, and S.-C. Zhang, Science **314**, 1757 (2006).
- ²⁹H. Zhang, C.-X. Liu, X.-L. Qi, X. Dai, Z. Fang, and S.-C. Zhang, Nat Phys **5**, 438 (2009).
- ³⁰C. Sabater, D. Gosálbez-Martínez, J. Fernández-Rossier, J. G. Rodrigo, C. Untiedt, and J. J. Palacios, Phys. Rev. Lett. **110**, 176802 (2013).